Pressure-stabilized structures of water-neon system under high pressure

Jurong Zhang,[1] Sen Shao,[2] and Hanyu Liu[3,*]

[1]*School of Physics and Electronics, Shandong Normal University, Jinan 250014, China*

[2]*Division of Physics and Applied Physics, School of Physical and Mathematical Sciences, Nanyang Technological University, Singapore*

[3]*State Key Laboratory of Superhard Materials and International Center for Computational Method & Software, College of Physics, Jilin University, Changchun 130012, China*

(Received 1 April 2022; revised 5 July 2022; accepted 18 July 2022; published 4 August 2022)

Neon (Ne), as the fifth most abundant element in the universe, is rare to react with other elements by forming stable solid compounds. It is well known that pressure is a powerful tool to generate the compounds that are inaccessible at ambient pressure. In this work, we performed structure-searching simulations to examine stable compounds of Ne and H_2O at a wide pressure range of 0–600 GPa. Our simulations identified two phases of H_2ONe and H_2ONe_2 under high pressure. By employing chemical-bonding analysis, interestingly, we found that Ne-O interactions are comparable in strength to that of conventional hydrogen bond. Moreover, our molecular dynamic simulations indicate the diffusion behavior of hydrogen atoms within a fixed Ne-O lattice framework of H_2ONe_2 at high pressure and high temperature. These results provide the implications for the possible existence of pressure-stabilized H_2ONe and H_2ONe_2 compounds viable in a variety of astronomical objects.

DOI: 10.1103/PhysRevB.106.054101

I. INTRODUCTION

Neon (Ne), whose *s* and *p* orbitals are fully occupied by electrons, is considered relatively inert and rather difficult to react with other elements. In an attempt to seek the stable Ne-bearing compounds, much effort has been devoted to the study of Ne-containing ions including Ne^+ [1], $(NeAr)^+$ [2], NeH^+ [3–5], and $(HeNe)^+$ [6] by spectroscopic and mass spectrometry analysis. However, there is the lack of any neutral molecules containing Ne atoms in these studies. Recently, pressure has been accepted as a useful way to help identify Ne-related compounds. For example, Ne hydrates are evidenced by experimental measurements at a relatively low pressure of ∼0.2 GPa [7] and ∼0.48 GPa [8]. Furthermore, several compounds are theoretically predicted to become stable under high pressure, such as $NeHe_2$ [9], alkali-oxides-Ne or sulfide-Ne [10], N-Ne [11,12], and H_2O-Ne compounds [7,8,13], while there is almost no chemical interaction between Ne and other atoms in these compounds. These results indicate that the search for stable Ne-bearing compounds is of great interest in the high-pressure community.

In recent studies, He was able to react with some elements by forming stable compounds at high pressures, e.g., H_2O [13–15], Na [16], MgF_2 [17], N [18,19] *et al.*, where pressure plays a critical role in stabilizing these unexpected compounds with novel physical properties, such as a superionic state at high temperatures. On the other hand, the recent theoretical studies further reveal that the stability of these compounds is intimately associated with electrostatic energy (Madelung energy). He and Ne are thought of as large voids to be inserted into these compounds without forming chemical bonds of any type, lowering the electrostatic energy of the system [17,20]. These studies leave an open question: could Ne react with H_2O by forming stable compounds at high pressures? In addition to the interests for high-pressure reaction between Ne and H_2O, both systems are possibly found in the interiors of some exoplanets, where high-pressure and high-temperature conditions may enhance the possibility of forming H_2O-Ne compounds.

In this regard, we here systematically explored the crystal structures of H_2O-Ne compounds at a wide pressure range of 0–600 GPa. As the result of simulations, we predicted two structures of H_2ONe_2 and H_2ONe under high pressure. Ne-O interaction for Fd-$3m$-H_2ONe_2 could be comparable in strength to that of conventional hydrogen bond. Moreover, our molecular dynamics simulations reveal the diffusion of hydrogen within a fixed Ne-O-lattice framework for H_2ONe_2, which is different from H_2OHe_2 where He atoms exhibit the diffusion behavior within a fixed H-O-lattice framework under high pressure and high temperature [15].

II. COMPUTATIONAL DETAILS

Extensive structure searches were conducted using a swarm-intelligence based CALYPSO (Crystal structure AnaLYsis by Particle Swarm Optimization) method and code [21,22], which is based on a global minimization of free-energy surfaces in conjunction with *ab initio* total-energy calculations and is widely used at high pressure [23–26]. Density-functional (DFT) theory calculations [27–29], the Perdew-Burke Ernzerhof [30] generalized gradient approximation [31] DFT, and frozen-core all-electron projector-augmented wave potentials [32] as performed with $1s$, $2s^2\,p^4$, and $2s^2\,p^6$ configurations treated as the valence electrons of H, O, and Ne in the VASP (Vienna *Ab initio* Simulation Package) code [33] are adopted in this work. The cutoff radius of the pseudopotentials for oxygen, hydrogen, and Ne were 0.820, 0.370, and 0.794 Å, respectively. The electronic

*Corresponding author: hanyuliu@jlu.edu.cn

wave functions were expanded in a plane-wave basis set with a kinetic energy cutoff of 1000 eV, and the Brillouin-zone (BZ) sampling was on k meshes [34] with a reciprocal-space resolution of $2\pi \times 0.032\,\text{Å}^{-1}$ to ensure that energies were converged to 1 meV/atom. The phonon calculations were performed with the PHONOPY code using a finite-displacement approach [35,36]. The bonding analysis is through the quantum theory of atoms in molecules approach (QTAIM) [37].

The *ab initio* molecular dynamics (AIMD) simulations were performed in the canonical (NVT) ensemble applying a Nosé thermostat [38]. Simulations reach 8 ps with 128 atoms of $I4_1md$-H_2ONe and 320 atoms of Fd-$3m$-H_2ONe_2. The time step was chosen to be 0.5 fs, and a $2 \times 2 \times 2$ k-mesh grid is used for the BZ sampling. We performed the simulations on the stable temperatures and pressure range as well as different possible states (solid, superionic, and liquid) of H_2ONe and H_2ONe_2.

We performed the molecular dynamics simulation with the temperatures range from 1000 to 5000 K with a temperature step of 500 K, and then we chose the temperature step in the regions of interest (500–1500 K and 2000–3500 K) to be 150 K to investigate the temperatures for phase transitions from the crystalline solid to the superionic phase, and then to the fluid. The Gibbs free energy (G) was calculated using the quasiharmonic approximation by the PHONOPY code. G is defined at a constant temperature (T) and pressure (P) by the formula $G(T,P) = \min_V[U(V) + PV + F_{\text{phonon}}(T,V)]$, where U is the internal lattice energy, V is volume, and F_{phonon} is the phonon free energy.$F_{\text{phonon}}(T,V) = K_BT \int_0^\infty g(\omega,V)\ln[2\sinh(\frac{\hbar\omega}{2K_BT})]d\omega$, where $g(\omega,V)$ is the phonon density of states at frequency ω. The minimal value of G was found at the equilibrium volume for a given T and P.

III. RESULTS

In this work, we first explored the high-pressure crystal structures of $(H_2O)Ne$, $(H_2O)Ne_2$, and $(H_2O)_2Ne$, with maximum simulation cells up to four formula units through the *ab initio* crystal structure search method. The convex hulls and the phase diagram of three stable stoichiometries are shown in Figs. 1(a)–1(d). For the reference systems to investigate the stability of predicted structures, we take the $I4_1/amd$ and $Pbcm$ phases for H_2O at 0–50 and 300–600 GPa [23,24], the Fm-$3m$ structure [25] for Ne at 0–600 GPa, the $Cmca$ structure for H_3O at 500 GPa [26], and the $Pbca$ structure for H_2O_2 at 500 GPa [27].

The stable structures of H_2O-Ne system are shown in Fig. 2. The $(H_2O)_2Ne$ stoichiometry was predicted to crystallize in trigonal structure (space group $P32$) from 1 bar to 1.2 GPa. $(H_2O)_2Ne$ phase adopted an orthorhombic structure [space group $Cmc21$ phase, 4 f.u. (formula units) per cell] from ∼1.2 to 13 GPa. After that, we found that the phase transition of $(H_2O)_2Ne$ is similar to previous studies [13]. Furthermore, H_2ONe is predicted to adopt a tetragonal structure (space group $I4_1md$ phase, 4 f.u. per cell) at a pressure range of ∼2–35 GPa as shown in Fig. 2(a). It is noted that the $I4_1md$-H_2ONe also adopted the same structure of H_2OHe compound [15], which has the same H_2O unit of $I4_1/amd$-VIII-H_2O and shows the similar H–O bonds and H-O-H angles. The length of H-O in H_2ONe is 1.00 Å, which is close to 0.99 Å in $I4_1/amd$ -VIII -H_2O at 5 GPa. The H-O-H angle of 106.36° in H_2ONe is larger than that (105.95°) in $I4_1/amd$-VIII-H_2O. These results indicate the presence of Ne is likely to weaken the interaction between H and O.

The H_2ONe_2 phase crystallizes in a cubic structure (space group Fd-$3m$ phase, 8 f.u. per cell) above 296 GPa. In this structure, each oxygen atom connects four hydrogen atoms by forming an O-H framework, where Ne atoms saturate in the center of O-H framework [Fig. 2(b)]. This structure has the same O-H framework of $Pbcm$-H_2O phase and Fd-$3m$-H_2OHe_2 phase. The H–O bond length of H_2ONe_2 is 1.08 Å, which is slightly larger than that (1.06 Å) in $Pbcm$-H_2O structure at 400 GPa. These bond lengths are all shorter than the sum of covalent radii 1.15 Å ($r_O = 0.37$ and $r_H = 0.68$), indicating a covalent H–O bonding. The H–O–H bond angle of H_2ONe_2 is 109.47°. We found that the Ne-Ne distance of 1.76 Å is shorter than the Ne-Ne van der Waals (vdW) bond length of 3.08 Å.

The electron localization functions (ELF) and electronic band structure of H_2ONe_2 are shown in Figs. 3(a) and 3(b). A calculated band gap of ∼15.48 eV for the Fd-$3m$-H_2ONe_2 phase reveals its insulator nature, which is similar to the previously predicted H_2O-He compound [14]. The ELF calculations indicate a covalent interaction between H and O atoms. We have also calculated the Bader charge of Ne, H, and O atoms for Fd-$3m$-H_2ONe_2 phase. On the basis, Ne atom gains 0.015e, O atom gains 1.35e, and H atom loses 0.69e.

To further analyze the interaction between Ne atom and other atoms of Fm-$3d$-H_2ONe_2 structure, we carried out quantum atoms in molecular (AIM) calculation analysis at 0 and 400 GPa as shown in Table I. The analysis of the electron density and its curvatures at a bond critical point (BCP), i.e., the saddle point along a bond path, could provide information about the type and properties of bonding. The AIM theory has been proven to be a useful tool for the characterization of interactions in closed-shell systems, such as ionic, hydrogen bonded, or vdW compounds. The calculated $\rho(r)$ at the BCPs are $0.355\,e^-\ \text{Å}^{-3}$ for the two nearest-neighbor Ne···O paths of Fm-$3d$-H_2ONe_2 phase at 400 GPa. The values of ρ(r) increase progressively at pressures from 300 to 400 GPa, as shown in Table II. The $\rho(r)$ for Fm-$3d$-H_2ONe_2 phase is $0.084\,e^-\ \text{Å}^{-3}$ at ambient pressure. To put this in perspective, the $\rho(r)$ for conventional hydrogen bonds fall in a range of 0.04 to $0.24\,e^-\ \text{Å}^{-3}$ at ambient pressure. It thus indicates that the strength of Ne···O interactions in the Fd-$3m$-H_2ONe_2 structure is comparable to or potentially stronger than conventional hydrogen bonds. The Laplacian $\nabla^2\rho(r)$ at the BCP are 1.58 and $8.13\,e^-\ \text{Å}^{-5}$ for the two nearest-neighbor Ne···O paths of Fm-$3d$-H_2ONe_2 phase at 0 and 400 GPa, which clearly defines closed-shell interactions between Ne and its nearest-neighbor O atoms. It is important for the $\nabla^2\rho(r)$ to be positive for the Ne···O interactions since these interactions are dominated by contraction of electrons away from the interatomic region toward each of the nuclei. It has been shown that the $\nabla^2\rho(r)$ of conventional hydrogen bonds falls in a range from 0.58 to $3.35\,e^-\ \text{Å}^{-5}$ [39]. Thus, the Ne···O interaction in the Fm-$3d$-H_2ONe_2 structure appears to be stronger than the conventional hydrogen bonding, which is consistent with the analysis of $\rho(r)$. The interaction of Ne···O in H_2ONe_2 is similar to He and O atoms in $Ibam$-$(H_2O)_2He$ [14] structures with $\rho(r)$ of $0.444\,e^-\ \text{Å}^{-3}$ and $\nabla^2\rho(r)$ of $9.215\,e^-\ \text{Å}^{-5}$. The

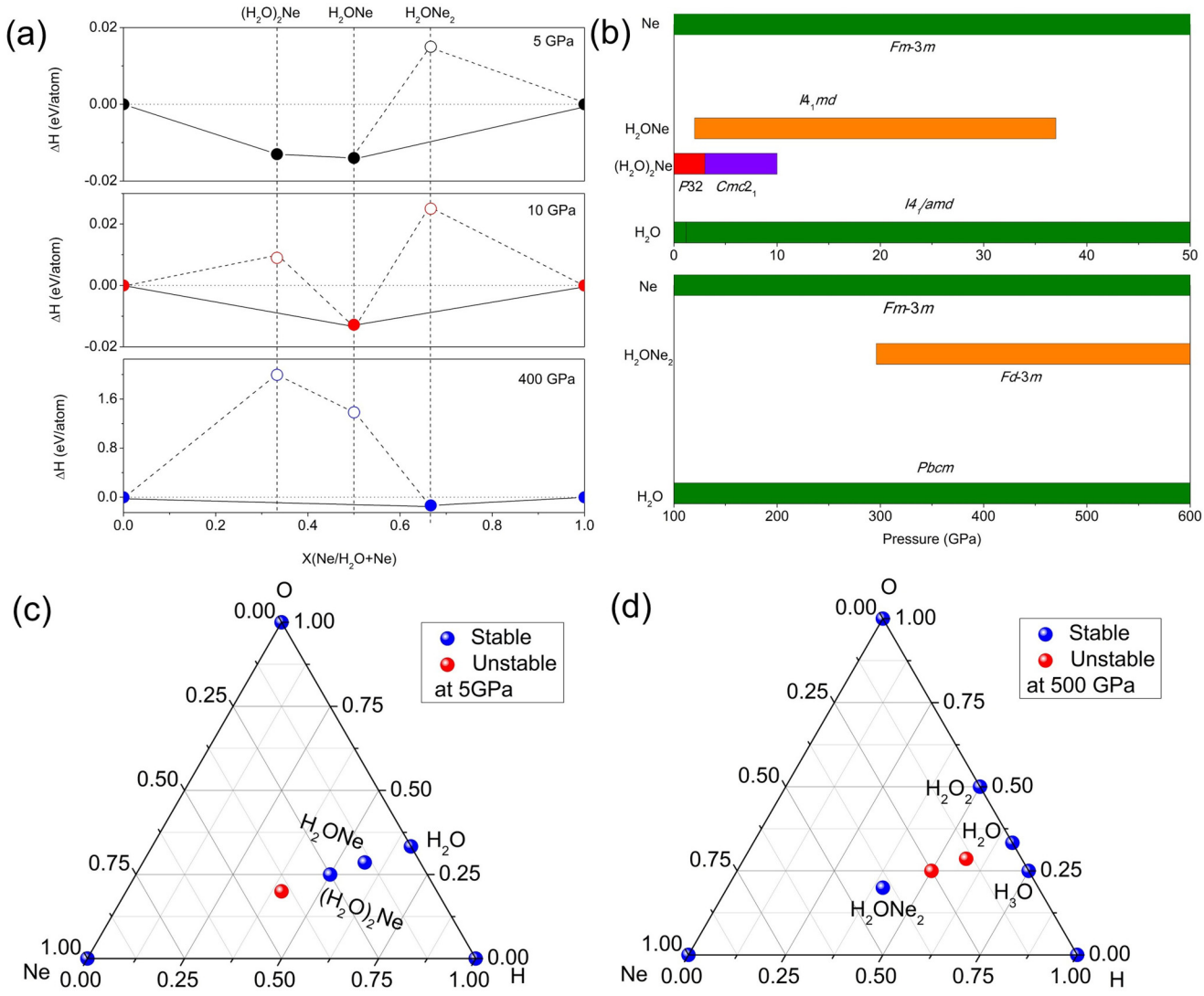

FIG. 1. Thermodynamics of the Ne-H_2O system of the stable compounds. (a) Convex hull for formation enthalpies (ΔH with respect to Ne and H_2O) at different pressures. (b) Pressure-composition phase diagram of the Ne-H_2O phases discovered in this work within zero-point energy, together with the previously known phases (green) in the pressure range of 0–50 and 100–600 GPa. (c) Ternary phase diagram of H-O-Ne system at 5 GPa. (d) Ternary phase diagram of H-O-Ne system at 500 GPa.

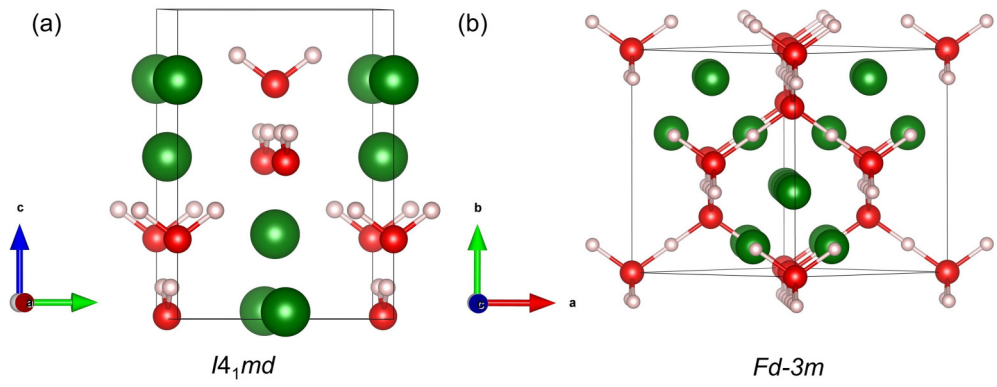

FIG. 2. Crystal structures of the stable compounds. (a) Crystal structures of $I4_1md$-H_2ONe. (b) Crystal structures of Fd-$3m$-H_2ONe_2. The detailed structural information are shown in Table III.

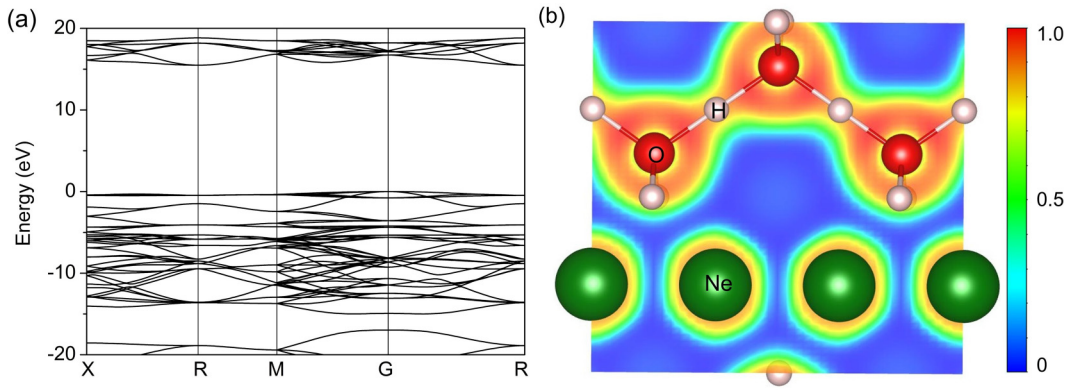

FIG. 3. Electronic properties of Fd-3m of H_2ONe_2. (a) Electronic band structure of Fd-3m-H_2ONe_2 at 400 GPa. (b) ELF of Fd-3m-H_2ONe_2 at 400 GPa.

BCP simulations of nearest Ne atoms also show that $\rho(r)$ is 0.596 e^- Å^{-3}, and $\nabla^2\rho(r)$ is 18.051e^- Å^{-5} with Ne-Ne distance of 1.762 Å at 400 GPa for Fm-3d-H_2ONe_2 structure, indicating the weak chemical association between Ne and Ne atom. With increasing pressure, we found that the $\rho(r)$ and $\nabla^2\rho(r)$ values between atoms increase, indicating the pressure could strengthen the interatomic interaction.

Ne is also detected in the Earth's interior from hot spots on the surface of the Earth and elevated ^{3}He / ^{4}He, ^{20}Ne / ^{22}Ne, and ^{36}Ar / ^{40}Ar ratios in some ocean island basalts, demonstrating the highly possible presence of primordial noble gases in the Earth's interior [40]. Moreover, Ne is possible to be created by decay or neutron capture of ^{25}Mg / ^{24}Mg series elements that have been trapped in the Earth's interior, where radiogenic ^{21}Ne and ^{22}Ne are found likely in the Earth's interior. In this regard, we further study the stability of H_2O-Ne compounds under high temperature and high pressure, as shown in Fig. 4. The stable region of $I4_1md$-H_2ONe agrees with the geotherm line, indicating $I4_1md$-H_2ONe may be stable in the deep Earth as well. Compared with the P-T phase diagrams of H_2OHe compounds reported previously, it is found that the transformation temperatures from solid state to superionic state and from superionic state to liquid state of $I4_1md$-H_2ONe and $I4_1md$-HOHe are almost the same. In addition, we found that the stable region of Fd-3m-H_2ONe_2 as shown does not correspond to the temperature and pressure curves of Uranus and Neptune.

The different states of matter were determined from *ab initio* molecular dynamics simulations and the mean-square displacement (MSD) of H_2ONe and H_2ONe_2 compounds. In order to show the structure state more clearly, MSD data and particle trajectory graph of Fd-m-H_2ONe compound are presented in Fig. 5. For the solid state, H, O, and Ne atoms are all at the balanced vibration position and the corresponding MSD data and atomic trajectory data at 53 GPa 3000 K are shown in Fig. 5(a). The MSD of atoms in solid state are straight lines as shown in Fig. 5(a), where black, red, and blue represent H, O, and Ne atoms, respectively. Their ion trajectories form clusters, where pink, red, and green represent trajectories of H, O, and Ne, respectively, as shown in Fig. 5(c). For superionic state, O and Ne atoms are at their balanced vibration position while H atoms move away from their equilibrium position and begin to diffuse freely at 55 GPa 4000 K as shown in Fig. 5(b). The black sloping line MSD of H atom increases with time in superionic state. The pink trajectory of H [Fig. 5(d)] is larger farther and out of its equilibrium vibration range. This result differs from the previous result for H_2OHe [15], in which the diffusion of He atoms is earlier than H atoms, probably because of the heavier Ne than He. For different material states of H_2ONe and H_2ONe_2, the corresponding temperature and pressure ranges are shown in Figs. 4(a) and 4(b). Learning from our P-T phase diagram, as the temperature and pressure increase, the H_2O-Ne compounds gradually changes from solid to superionic and then to liquid.

TABLE I. Topological properties of the BCP at the shortest Ne···Ne and Ne···O contacts (strong closed-shell interactions) for the Fd-3m-H_2OHe_2 structure at 400 GPa.

Bond type	d (Å)	$\rho(r_{BCP})$ (e^- Å^{-3})	$\nabla\rho(r_{BCP})$ (e^- Å^{-5})
Hydrogen bonds [39]		0.04–0.24	0.58–3.35
He–O [14]	1.773	0.444	9.215
Ne–Ne at 400 GPa	1.762	0.596	18.051
Ne–O at 400 GPa	2.067	0.355	8.127
Ne–Ne at 0 GPa	2.277	0.136	3.405
Ne–O at 0 GPa	2.670	0.084	1.580

TABLE II. Topological properties of the BCP at the shortest Ne···Ne and Ne···O contacts (strong closed-shell interactions) for the Fd-3m-H_2OHe_2 structure at 400 GPa.

Bond type	d(Å)	$\rho(r_{BCP})$ (e^-Å^{-3})	$\nabla^2\rho(r_{BCP})$ (e^-Å^{-5})
Hydrogen bonds		0.04-0.24	0.58-3.35
Ne-Ne at 300 GP	1.812	0.512	15.419
Ne-Ne at 400 GPa	1.762	0.596	18.051
Ne-O at 300GPa	2.125	0.306	6.805
Ne-O at 400GPa	2.067	0.355	8.127
He-O	1.773	0.444	9.215

TABLE III. Predicted structural parameters of various H_2O-Ne compounds.

Compound	Pressure (GPa)	Space group	Lattice Parameters(Å,deg)	Atomic coordinates			
				Atom	x	y	z
H_2ONe	5 GPa	$I4_1md$	$a=b=4.437$	8b	0.500	−0.320	−0.146
			$c=6.293$	4a	0.500	−0.500	0.758
			$\alpha=\beta=\gamma=90$	4a	1.000	−0.000	0.771
H_2ONe_2	400 GPa	Fd-3m	$a=b=c=4.9846$	16c	0.375	0.125	0.375
			$\alpha=\beta=\gamma=90$	8a	1.000	0.500	0.500
				16d	0.875	0.125	0.375

IV. CONCLUSION

In summary, we predicted two compounds of H_2ONe and H_2ONe_2 by swarm intelligence structure simulations. The predicted stable high-pressure phase of $I4_1md$-H_2ONe is stable from about 2 to 35 GPa and Fd-3m-H_2ONe_2 phase is stable from 300 to 600 GPa. High-temperature and -pressure phase diagram analysis shows that $I4_1md$-H_2ONe may be stable in the Earth's interior. The Fd-3m-H_2ONe_2 phase is an insulator with an indirect band gap of ∼15.48 eV at 400 GPa. The ELF, Bader, and AIM analysis of Fd-3m-H_2ONe_2 at 400 GPa suggest that Ne-Ne and Ne-O have the chemical association, the strength of which is similar to the hydrogen bonds in dense ice phases.

ACKNOWLEDGMENTS

This work is supported by the National Natural Science Foundation of China (Grants No. 12147135 and No. 12074138), Postdoctoral Science Foundation of China (Grant No. 2021M691980), and Natural Science Foundation of Shandong Province (Grant No. ZR202103010004).

APPENDIX

We have also calculated the Born effective charge for the predicted compounds. The results show that the Born effective charge of H and O atoms is close to ion charge, while the Born effective charge of neon is small (Table IV), indicating that there is polarization between H and O atoms while Ne remains electrically neutral.

Further phonon calculations show that there is no imaginary frequency in the whole Brillouin region for the predicted structures of H_2ONe_2 and H_2ONe, indicating that these structures are dynamically stable, as shown in Fig. 6 We also wish to point out that this kind of phonon calculations could not provide any implication for the further understanding of dynamical properties for superionic and liquid states of these predicted structures at high temperatures, which encourages us to perform further molecular dynamics simulations as we will discuss them later.

The equation of state of H_2O-Ne, H2O and Ne are shown in Fig.7. The volume of the crystal decreases with increasing pressure. In comparison, the volume of H_2O and Ne changes with pressure more gently than that of H_2ONe and H_2ONe_2.

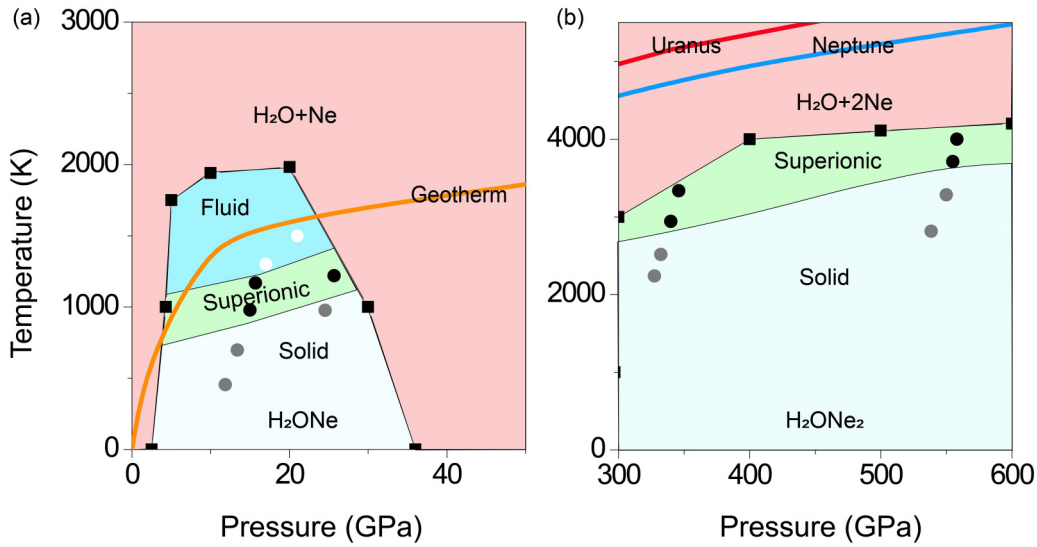

FIG. 4. Pressure-temperature phase diagram of H_2ONe and H_2ONe_2. (a) Stability fields separating H_2O+Ne of $I4_1md$-H_2ONe compounds. (b) Stability fields separating H_2O+Ne of Fm-3d-H_2ONe_2 compound. Solid (white), superionic (green), liquid (blue) phases, and unstable (pink) of H_2ONe and H_2ONe_2 compounds, obtained from AIMD simulations. Temperature and pressure curve inside Earth [41]; Uranus and Neptune [42] are shown as orange, red, and blue lines.

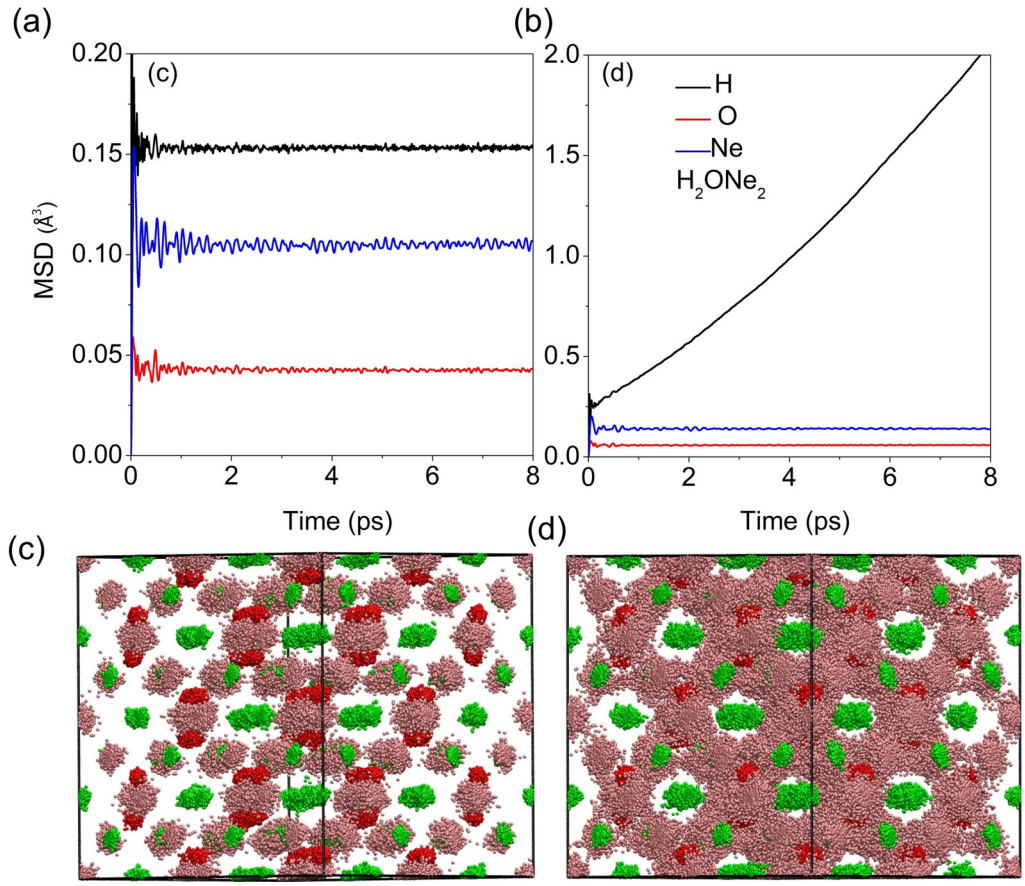

FIG. 5. Behavior of H and Ne atoms compared to O atoms in *Fd*-3*m* H_2ONe_2 from AIMD simulations at 3000 and 4000 K. (a) Averaged MSDs for the H, O, and Ne atoms of *Fd*-3*m*-H_2ONe_2 from AIMD simulations at 3000 K and 53 GPa. (b) Averaged MSDs for the H, O, and Ne atoms of *Fd*-3*m*-H_2ONe_2 from AIMD simulations at 4000 K and 55 GPa. (c) Atomic trajectories of the *Fd*-3*m*-H_2ONe_2 solid phase (3000 K, 53 GPa). (d) Superionic H phase (4000 K, 55 GPa).

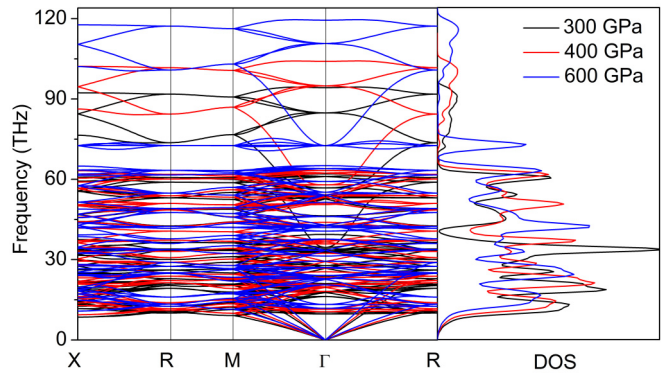

FIG. 6. Calculated phonon dispersion and density of states (DOS) curves of H_2ONe_2 at 300 GPa, 400 GPa and 600 GPa.

TABLE IV. The calculated Born effective charge tensor of *Fd*-3*m*-H_2ONe_2 at 400 GPa.

	Z*/e								
Atoms	Z_{xx}	Z_{xy}	Z_{xz}	Z_{yx}	Z_{yy}	Z_{yz}	Z_{zx}	Z_{zy}	Z_{zz}
H	1.035	−0.626	0.626	−0.626	1.035	−0.626	0.626	−0.626	1.035
O	−1.820	0.000	0.000	0.000	−1.820	0.000	0.000	0.000	−1.820
Ne	−0.125	−0.061	0.061	−0.061	−0.125	−0.061	0.061	−0.061	−0.125

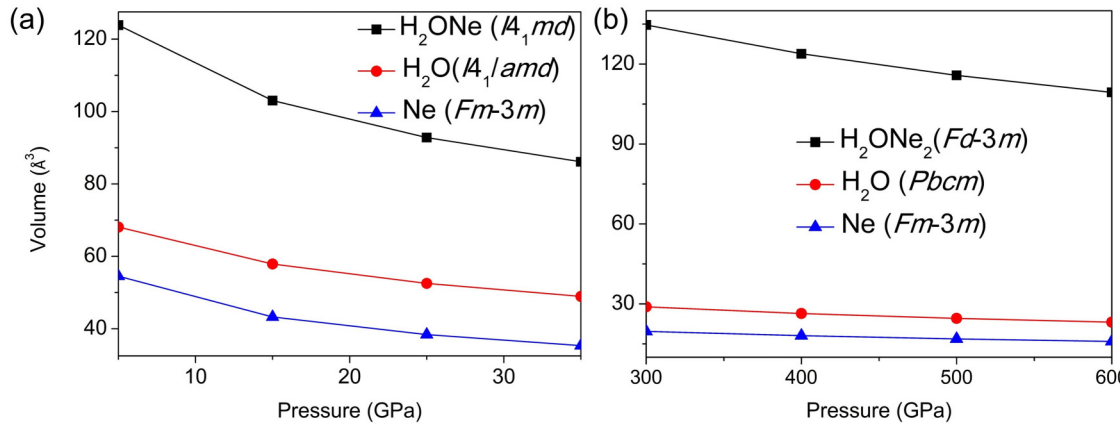

FIG. 7. The equation of state. (a) The equation of state of H_2ONe-$I4_1md$, H_2O-$I4_1/amd$ and Ne-*Fm*-3*m*. (b) The equation of state of H_2ONe_2-*Fd*-3*m*, H_2O-*Pbcm* and Ne-*Fm*-3*m*.

[1] A. M. Covington, A. Aguilar, I. R. Covington, M. F. Gharaibeh, G. Hinojosa, C. A. Shirley, R. A. Phaneuf, I. Álvarez, C. Cisneros, I. Dominguez-Lopez *et al.*, Photoionization of Ne^+ using synchrotron radiation, Phys. Rev. A **66**, 062710 (2002).

[2] S. T. Pratt and P. M. Dehmer, Photoionization of the neon–rare gas dimers NeAr, NeKr, and NeXe, J. Chem. Phys. **76**, 3433 (1982).

[3] J. Lorenzen, H. Morgner, W. Bussert, M.-W. Ruf, and H. Hotop, Ionization of hydrogen and deuterium atoms in thermal energy collisions with state-selected Ne ($3s^3$ P_2, $^3P_0$) metastable atoms, Z. Phys. A: Atoms Nuclei **310**, 141 (1983).

[4] J. Johns, Spectra of the protonated rare gases, J. Mol. Spectrosc. **106**, 124 (1984).

[5] M. Wong, P. Bernath, and T. Amano, Observation of the infrared absorption spectra of $^{20}Ne\,H^+$ and $^{22}Ne\,H^+$ with a difference frequency laser, J. Chem. Phys. **77**, 693 (1982).

[6] I. Dabrowski and G. Herzberg, The spectrum of $HeNe^+$, J. Mol. Spectrosc. **73**, 183 (1978).

[7] Y. A. Dyadin, É. G. Larionov, E. Y. Aladko, A. Y. Manakov, F. V. Zhurko, T. V. Mikina, V. Y. Komarov, and E. V. Grachev, Clathrate formation in water-noble gas (hydrogen) systems at high pressures, J. Struct. Chem. **40**, 790 (1999).

[8] X. Yu, J. Zhu, S. Du, H. Xu, S. C. Vogel, J. Han, T. C. Germann, J. Zhang, C. Jin, and J. S. Francisco, Crystal structure and encapsulation dynamics of ice II-structured neon hydrate, Proc. Natl. Acad. Sci. USA **111**, 10456 (2014).

[9] P. Loubeyre, M. Jean-Louis, R. LeToullec, and L. Charon-Gérard, High Pressure Measurements of the He-Ne Binary Phase Diagram at 296 K: Evidence for the Stability of a Stoichiometric $Ne(He)_2$ Solid, Phys. Rev. Lett. **70**, 178 (1993).

[10] H. Gao, J. Sun, C. J. Pickard, and R. J. Needs, Prediction of pressure-induced stabilization of noble-gas-atom compounds with alkali oxides and alkali sulfides, Phys. Rev. Mater **3**, 015002 (2019).

[11] T. Plisson, G. Weck, and P. Loubeyre, $(N_2)_6Ne_7$: A High Pressure van Der Waals Insertion Compound, Phys. Rev. Lett. **113**, 025702 (2014).

[12] M. Kooi and J. Schouten, High-pressure Raman investigation of mutual solubility and compound formation in Xe-N_2 and Ne-N_2, Phys. Rev. B. **60**, 12635 (1999).

[13] P. Teeratchanan and A. Hermann, Computational phase diagrams of noble gas hydrates under pressure, J. Chem. Phys. **143**, 154507 (2015).

[14] H. Liu, Y. Yao, and D. D. Klug, Stable structures of He and H_2O at high pressure, Phys. Rev. B. **91**, 014102 (2015).

[15] C. Liu, H. Gao, Y. Wang, R. J. Needs, C. J. Pickard, J. Sun, H.-T. Wang, and D. Xing, Multiple superionic states in helium–water compounds, Nat. Phys. **15**, 1065 (2019).

[16] X. Dong, A. R. Oganov, A. F. Goncharov, E. Stavrou, S. Lobanov, G. Saleh, G.-R. Qian, Q. Zhu, C. Gatti, and V. L. Deringer, A stable compound of helium and sodium at high pressure, Nat. Chem. **9**, 440 (2017).

[17] Z. Liu, J. Botana, A. Hermann, S. Valdez, E. Zurek, D. Yan, H.-q. Lin, and M.-s. Miao, Reactivity of He with ionic compounds under high pressure, Nat. Commun. **9**, 951 (2018).

[18] W. Vos, L. Finger, R. Hemley, J. Hu, H. Mao, and J. Schouten, A high-pressure van der Waals compound in solid nitrogen-helium mixtures, Nature (London) **358**, 46 (1992).

[19] Y. Li, X. Feng, H. Liu, J. Hao, S. A. Redfern, W. Lei, D. Liu, and Y. Ma, Route to high-energy density polymeric

nitrogen *t*-N via He−N compounds, Nat. Commun. **9**, 722 (2018).

[20] M. Miao, Y. Sun, H. Liu, and Y. Ma, Open questions on the high-pressure chemistry of the noble gases, Commun. Chem. **5**, 1 (2022).

[21] Y. Wang, J. Lv, L. Zhu, and Y. Ma, Crystal structure prediction via particle-swarm optimization, Phys. Rev. B. **82**, 094116 (2010).

[22] Y. Wang, J. Lv, L. Zhu, and Y. Ma, CALYPSO: A method for crystal structure prediction, Comput. Phys. Commun. **183**, 2063 (2012).

[23] J. Zhang, G. Chen, and H. Liu, Stable structures and superconductivity in a Y–Si system under high pressure, J. Phys. Chem. Lett. **12**, 10388 (2021).

[24] H. Liu, I. I. Naumov, R. Hoffmann, N. Ashcroft, and R. J. Hemley, Potential high-Tc superconducting lanthanum and yttrium hydrides at high pressure, Proc. Natl. Acad. Sci. USA **114**, 6990 (2017).

[25] H. Wang, S. T. John, K. Tanaka, T. Iitaka, and Y. Ma, Superconductive sodalite-like clathrate calcium hydride at high pressures, Proc. Natl. Acad. Sci. USA **109**, 6463 (2012).

[26] J. Zhang, H. Liu, Y. Ma, and C. Chen, Direct H-He chemical association in superionic FeO_2H_2He at deep-earth conditions, Natl. Sci. Rev. **9**, nwab168 (2022).

[27] W. Kohn, A. D. Becke, and R. G. Parr, Density functional theory of electronic structure, J. Phys. Chem. **100**, 12974 (1996).

[28] W. Kohn and L. J. Sham, Self-consistent equations including exchange and correlation effects, Phys. Rev. **140**, A1133 (1965).

[29] P. Hohenberg and W. Kohn, Inhomogeneous electron gas, Phys. Rev. **136**, B864 (1964).

[30] J. P. Perdew and Y. Wang, Accurate and simple analytic representation of the electron-gas correlation energy, Phys. Rev. B **45**, 13244 (1992).

[31] J. P. Perdew, K. Burke, and M. Ernzerhof, Generalized Gradient Approximation Made Simple, Phys. Rev. Lett. **77**, 3865 (1996).

[32] P. E. Blöchl, Projector augmented-wave method, Phys. Rev. B. **50**, 17953 (1994).

[33] G. Kresse and J. Furthmüller, Efficient iterative schemes for ab initio total-energy calculations using a plane-wave basis set, Phys. Rev. B. **54**, 11169 (1996).

[34] H. J. Monkhorst and J. D. Pack, Special points for Brillouin-zone integrations, Phys. Rev. B. **13**, 5188 (1976).

[35] K. Parlinski, Z. Q. Li, and Y. Kawazoe, First-Principles Determination of the Soft Mode in Cubic ZrO_2, Phys. Rev. Lett. **78**, 4063 (1997).

[36] A. Togo, F. Oba, and I. Tanaka, First-principles calculations of the ferroelastic transition between rutile-type and $cacl_2$-type SiO_2 at high pressures, Phys. Rev. B. **78**, 134106 (2008).

[37] R. F. W. Bader, Atoms in molecules, Acc. Chem. Res. **18**, 9 (1985).

[38] S. Nosé, A unified formulation of the constant temperature molecular dynamics methods, J. Chem. Phys. **81**, 511 (1984).

[39] U. Koch and P. L. Popelier, Characterization of CHO hydrogen bonds on the basis of the charge density, J. Phys. Chem. **99**, 9747 (1995).

[40] Z. Xiong, T. Tsuchiya, and J. A. Van Orman, Helium and argon partitioning between liquid iron and silicate melt at high pressure, Geophys. Res. Lett. **48**, e2020GL090769 (2021).

[41] S. Anzellini, A. Dewaele, M. Mezouar, P. Loubeyre, and G. Morard, Melting of iron at earth's inner core boundary based on fast X-ray diffraction, Science **340**, 464 (2013).

[42] R. Redmer, T. R. Mattsson, N. Nettelmann, and M. French, The phase diagram of water and the magnetic fields of Uranus and Neptune, Icarus **211**, 798 (2011).